Int. J. Electrochem. Sci., 13 **(2018)** 12010 – 12023, doi: 10.20964/2018.12.48

International Journal of
ELECTROCHEMICAL
SCIENCE
www.electrochemsci.org

Corrosion Protection of Water-borne Epoxy Coatings Incorporated with Graphene

Mingjun Cui[1], *Jianda Dong*[2], *Kaihe Zhou*[2], *Yunhui Fang*[2], *Jibin Pu*[3], *Haichao Zhao*[3,*], *Yonggang Wang*[1,4*], *Liping Wang*[3]

[1] Key Laboratory of Impact and Safety Engineering, Ministry of Education of China, Ningbo University, Ningbo 315211, China
[2] State Grid Zhejiang Electric Power Corporation Ningbo Power Supply Company Co., Ltd, Ningbo 315201, China
[3] Key Laboratory of Marine Materials and Related Technologies, Zhejiang Key Laboratory of Marine Materials and Protective Technologies, Ningbo Institute of Materials Technology and Engineering, Chinese Academy of Sciences, Ningbo 315201, China
[4]State Key Laboratory of Explosion Science and Technology, Beijing Institute of Technology, Beijing, China
[*]E-mail: zhaohaichao@nimte.ac.cn, wangyonggang@nbu.edu.cn

Received: 18 June 2018 / *Accepted:* 5 August 2018 / *Published:* 5 November 2018

In present study, phenosafranin (PSF) was employed to achieve the dispersion of graphene in water owing to the presence of π-π interaction which was also confirmed from the absorption free energy calculated by first principles based on density functional theory. In addition, water-borne epoxy (WEP) coatings containing graphene, PSF and PSF@G were prepared and fabricated on the electrodes. Meanwhile, the corrosion protection performance of different coatings during the immersion in 3.5 wt% NaCl solution was investigated and compared. It could be concluded from the results that PSF@G/WEP coating presented better protective performance than other coatings since the well dispersed graphene in WEP provided superior impermeability to corrosive medium. Besides, the PSF surfactant used to disperse graphene was also beneficial to improve the protective performance of the WEP coating.

Keywords: Graphene, Phenosafranin, π-π interaction, Water-borne epoxy, Corrosion protection

1. INTRODUCTION

Graphene, one of two-dimensional (2D) material, has been widely investigated in many fields owing to their unique structure and excellent properties, such as high electrical property [1-3], high

thermal conductivity [4-6] and strong chemical inertness [7]. Especially, the impermeability to all gases and corrosive medium makes graphene an ideal candidate as protective coatings [8, 9]. Besides, graphene nanosheets can also act as one component to improve the anticorrosive performance of polymeric coatings [10-13]. However, there is weak van der Waals interaction between adjacent graphene layers, which plays an important role on the dispersion status of graphene to a large extent. Hence, incorporating graphene into such a polymeric coating is still a challenge. Particularly, with the increasing environmental awareness, the use of water-borne polymeric coating becomes imperative. Thus, achieving the aqueous exfoliation of graphene is the key to develop the anticorrosive water-borne polymeric coating.

Several methods have been explored for the production of graphene, such as mechanical method, epitaxial growth [14], chemical vapor deposition (CVD) [15-17], the reduction of graphene oxide [18-20] and liquid-phase exfoliation [21-26]. Many researches focused on the functionalization of graphene oxide to achieve the dispersion of graphene in water and the anticorrosion applications [13, 27-29]. However, the residual defects caused by the reduction of graphene oxide lead to the degradation of the properties. In contrast, graphene nanosheets produced from liquid-phase exfoliation method exhibit a high quality and excellent properties [22, 30]. Great efforts have been done to improve the dispersion of the graphene nanosheets in aqueous solution by using effective surfactants. Zhang and coworkers designed an effective surfactant with electron-deficient π-conjugated unit and achieved the exfoliation of graphene in aqueous solution [23]. Ma and coworkers reported that the addition of a small amount of ammonia solution could exfoliate the pristine graphite to few-layer graphene nanosheets while the concentration of graphene dispersions was only 0.058 mg/mL [22]. Besides, pyrene-conjugated hyaluronan (Py-HA) could also be used to facilitate the exfoliation of graphite in water through the π-π stacking interactions [21].

However, most of the anticorrosion applications of graphene with liquid-phase exfoliation method in water-borne polymeric coatings have been rarely researched. Therefore, in this research, we report a new aromatic surfactant (phenosafranin, PSF) to achieve the dispersion of graphene in water owing to the presence of π-π interaction, and the corrosion protection of corresponding graphene/water-borne epoxy composite coating for carbon steel during the exposure in 3.5 wt% NaCl solution is also investigated by electrochemical measurements and salt spray test.

2. EXPERIMENTS

2.1 Materials

Sodium chloride was purchased from Sinopharm Chemical Reagent Beijing Co., Ltd. Phenosafranin (PSF) was purchased from Aladdin Industrial Corporation. Graphene was provided by Ningbo Morsh Tech Co., Ltd. Epoxy resin (E51, the epoxide number: 0.5, solid content: 98%) and waterborne curing agents (epoxide equivalent: 293, solid content: 60%) were provided by Hangzhou Hanma Paint &Coatings Co., Ltd. Q235 carbon steel (1×1×1 cm^3) was used for the corrosion investigation.

2.2 Preparation of Graphene Dispersions

50 mg of PSF was first dissolved completely in 10 mL of deionized water. Then 50 mg of graphene was added into the above mixture and dispersed with ultrasonication for 1 h to obtain a uniform G@PSF dispersion.

2.3 Preparation of Graphene/epoxy Composite Coatings

During the preparation process, 2.94 g of waterborne curing agent was added into the PSF@G dispersion and mixed uniformly with magnetic stirring for 2 h. Then, the mixture was heated to remove the residual water. Subsequently, 1.96 g of E51 epoxy resin was added into the above mixture and stirred 30 min. Then two drops of water-borne defoamer were added to remove the bubbles in the above mixture. Eventually, the mixture was coated on the Q235 carbon steel surface by wire bar coater with the thickness of 50 μm and cured at room temperature for 24 h. The obtained coating was named as PSF dispersed graphene/water-borne epoxy composite coating (PSF@G/WEP). As a comparison, blank water-borne epoxy coating (WEP), graphene/water-borne epoxy composite coating (G/WEP) and PSF/water-borne epoxy composite coating (PSF/WEP) were also prepared with same process.

2.4 Characterization and measurement

2.4.1 Characterization

The surface morphology of graphene before and after dispersion was estimated by scanning electron microscopy (SEM, S4800, Hitachi, Japan), transmission electron microscopy (TEM, Tecnai F20, USA) and scanning probe microscopy (SPM Vecco, Dimension 3100, USA). The fracture surface of the coatings was examined by scanning electron microscopy (SEM, S4800, Hitachi, Japan). Before the SEM test, Au was sputtered to improve the conductivity of the coatings.

2.4.2 Electrochemical measurements

In this investigation, electrochemical measurements were conducted using CHI-660E electrochemical work station with a classical three-electrode electrochemical system. A saturated calomel electrode (SCE) was used as reference electrode (RE), a platinum sheet electrode was used as counter electrode (CE) and the prepared specimen with 1 cm^2 of exposed area was used as working electrode (WE). Before each test, open circuit potential (OCP) was recorded to check whether the system reached a steady status. At different immersion time, electrochemical impedance spectroscopy (EIS) was performed at OCP over the frequency range of 100 kHz to 10 mHz with a 20 mV of sinusoidal perturbations. After that, Zview software was used for fitting the EIS results. All tests were repeated three times to ensure reproducibility.

3. RESULTS AND DISCUSSION

3.1 The dispersion of graphene in water

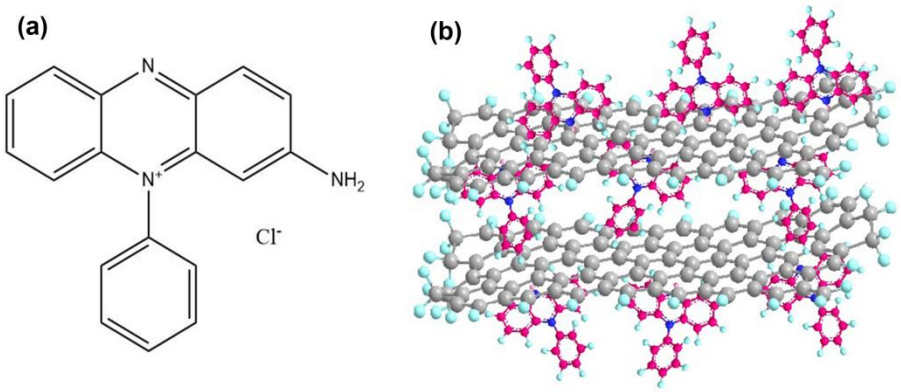

Figure 1. (a) The chemical structure of PSF and (b) corresponding dispersion mechanism of graphene

In this study, a surfactant-PSF using to disperse the graphene in water was reported. As shown in Fig. 1, PSF is an ionic organic salt with large electron-deficient π-conjugated aromatic system, which makes it possible to absorb on the graphene surface via π-π and Coulomb interactions, thus modifying the hydrophily of the graphene.

Table 1. Absorption free energy of surfactants on the graphene surface estimated by periodic DFT calculations

Sample	Chemical structure	Absorption free energy on the graphene surface (eV)
SDBS	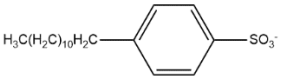	-0.273
PSA	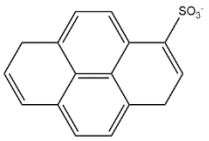	-0.439
PSF	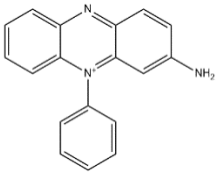	-0.7

To confirm the above hypothesis, the adsorption free energy of surfactant-PSF on graphene surface is calculated by first principles based on density functional theory. In general, adsorption energies (E_{ads}) for all possible adsorbates can be calculated according to the equation $E_{ads} = E_{system} - (E_{graphene} + E_{molecule})$, where E_{system}, $E_{graphen}$ and $E_{molecule}$ are total energies of the adsorbed species on graphene, the clean graphene surface, and the corresponding PSF molecule, respectively [23]. The larger the adsorption energy is, the stronger affinity of the PSF molecule to the

graphene surface is. The obtained result is also compared with previous reports. Their chemical structures and absorption free energies on the graphene surface are shown in Table 1. PSA and SDBS were commonly used to disperse carbon nanomaterials (SWCNT, graphene) [23]. In comparison, PSF has larger adsorption free energy than PSA and SDBS, implying the strong affinity between PSF and graphene, which may be ascribed to the large, electron-deficient π-conjugated aromatic system of PSF.

Accompanying with ultrasonication, graphene nanosheets are uniformly dispersed into the water in presence of PSF. In order to directly observe the dispersion status of graphene, the dispersion images after 12 h of storage are recorded in Fig. 2. Graphene nanosheets are easily adhered on the bottle wall when directly dispersed in water. Further, obvious sediments are observed in the bottom of bottle (Fig. 2a_1-a_2). In contrast, the dispersion of graphene nanosheets in water is relatively uniform with the assistance of PSF and there is no obvious adhesion and sediments in the wall and bottom of bottle, as shown in Fig. 2b_1-b_2. The reason for this phenomenon is that water-soluble PSF can absorb on the graphene surface via strong π-π interaction, thus leading to the uniform dispersion of graphene nanosheets in water, which is consistent with the calculated result.

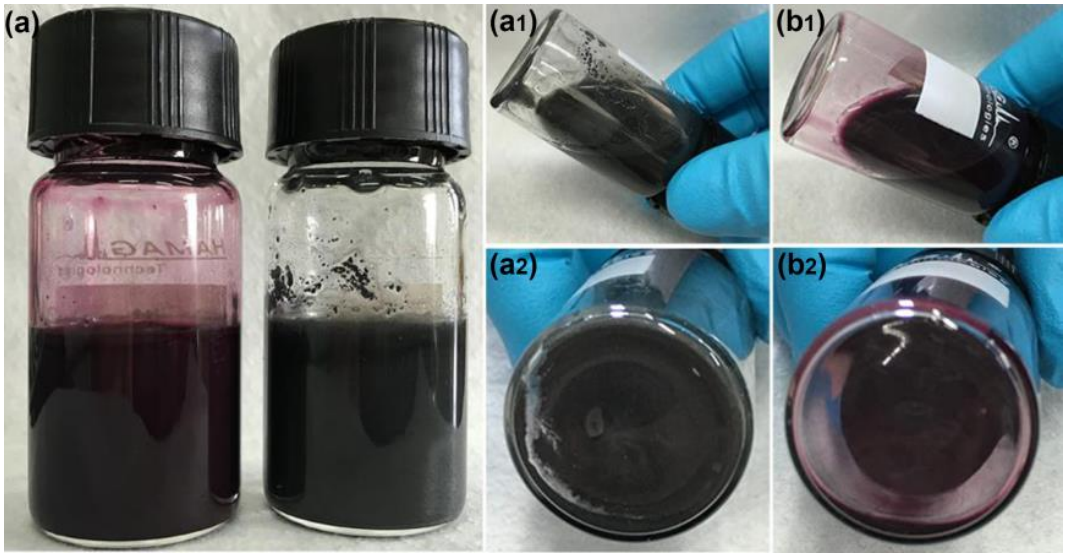

Figure 2. (a) The dispersion of G and PSF@G in water, (a_1/a_2) pristine graphene and (b_1/b_2) PSF@G

Further, the dispersion morphologies of the graphene nanosheets in the absence and presence of PSF are also checked by SEM and TEM. The graphene and PSF@G dispersions are dripped respectively on the silicon substrates and dried before SEM analysis. It can be observed from Fig. 3a that the graphene nanosheets dispersed directly in water mainly exist in the form of thick layers and have large specific surface area. By comparison, the thickness of graphene nanosheets in PSF@G dispersions becomes thinner than that in graphene dispersions, indicating the well exfoliation of graphene nanosheets (Fig. 3b). As shown in Fig. 3c, PSF@G nanosheets consist of few layers and appear to be transparent under electron beam. Owing to the absorption of PSF on graphene surface, some small black dots can be observed on the PSF@G surface when the image is magnified (Fig. 3d-e). SPM result in Fig. 4 shows that the thickness of the PSF@G nanosheets is approximate 3~4 nm (~10 layers), indicating the well exfoliation of graphene nanosheets.

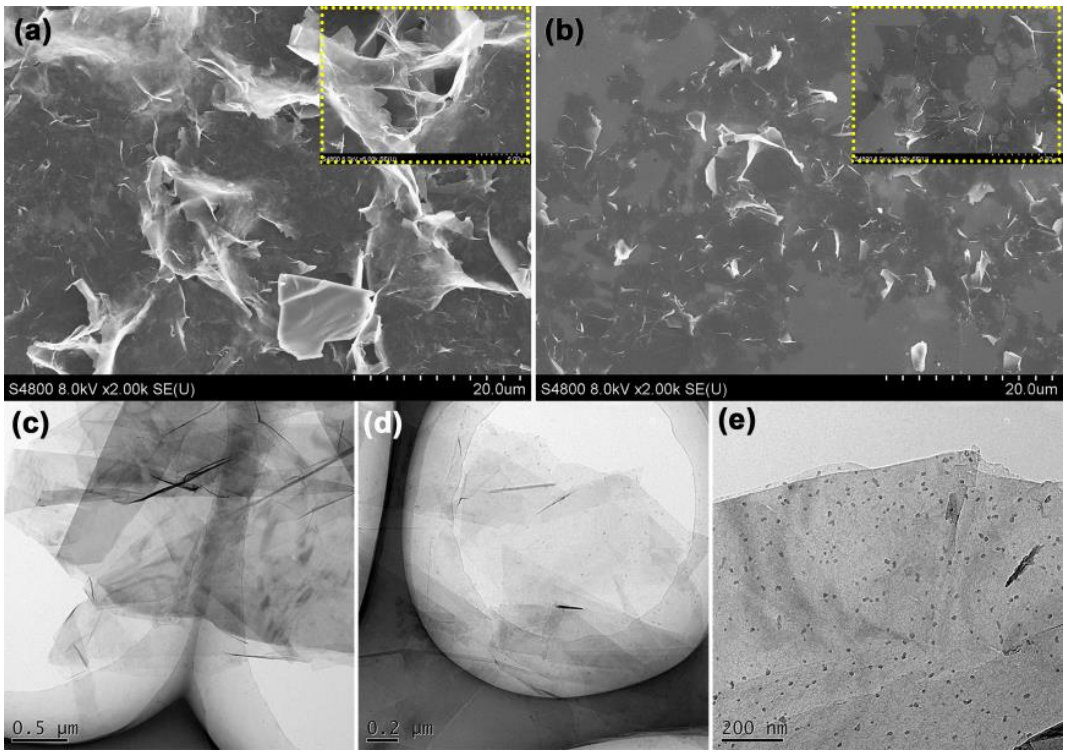

Figure 3. The SEM images for (a) direct dispersed graphene and (b) PSF@G, and (c-e) TEM images of PSF@G

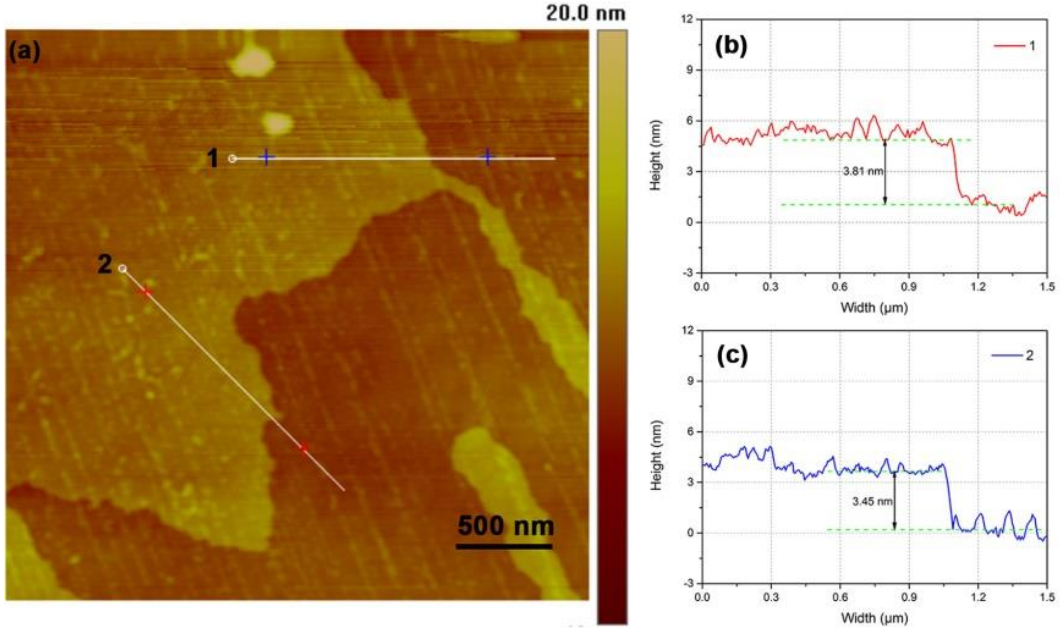

Figure 4. (a) SPM morphology and (b/c) height profile of the PSF@G

According to the above results, it can be safe to conclude that graphene can be dispersed uniformly in water with the assistance of PSF, which will be beneficial to achieve the application of graphene in water-borne epoxy coating.

3.2 Corrosion protection of graphene/water-borne epoxy composite coatings

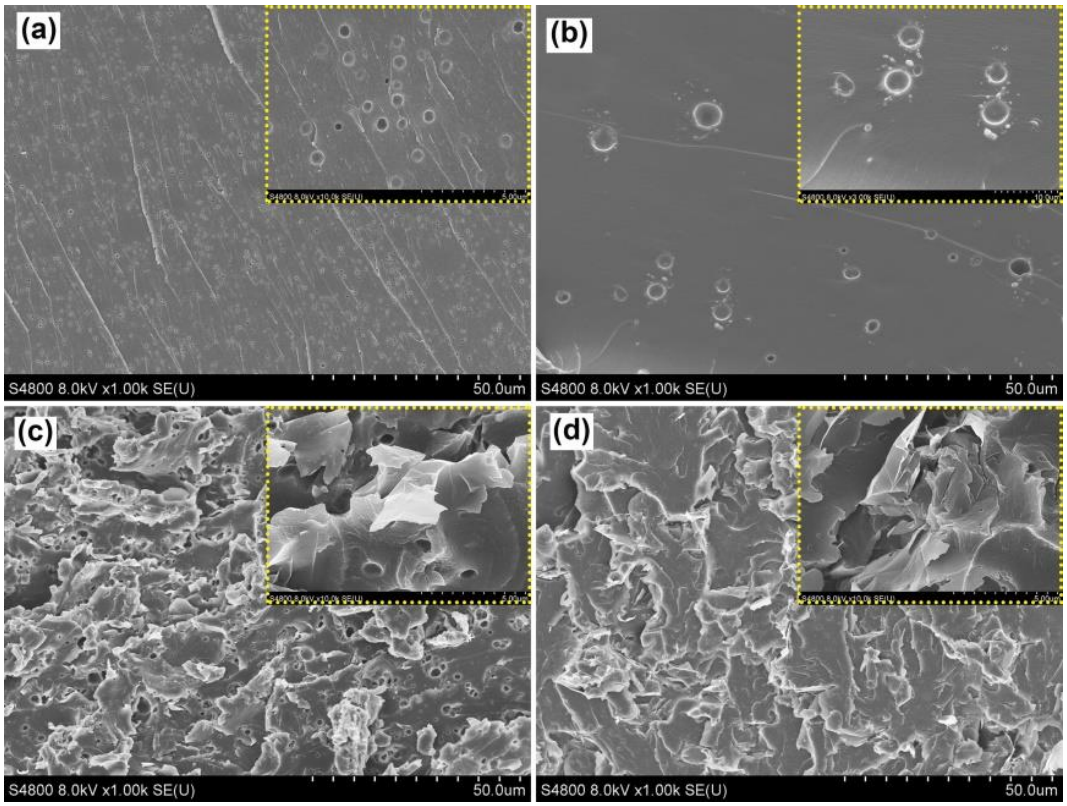

Figure 5. The fracture surface morphologies of different coatings, (a) WEP coating, (b) PSF/WEP coating, (c) G/WEP coating and (d) PSF@G/WEP coating

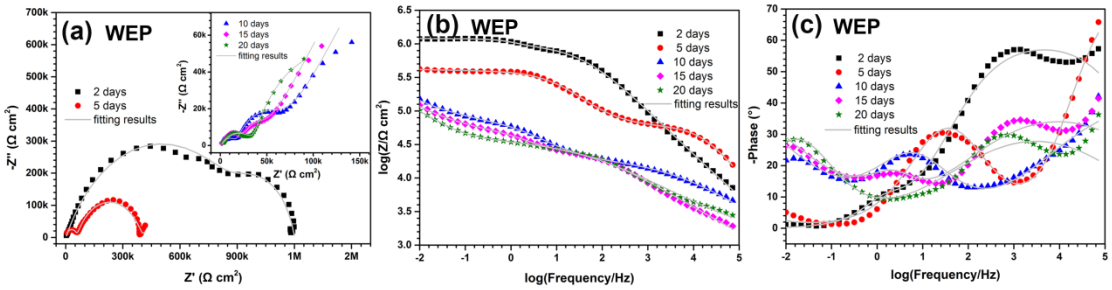

Figure 6. EIS results of WEP coating during 20 days of immersion in 3.5 wt% NaCl solution, (a) Nyquist plot, (b) Bode plot (Impedance modulus ~ Frequency) and (c) Bode plot (–Phase angle ~ Frequency), the scatter in the plot is experimental data and the solid line is the fitting results

In general, the corrosion protection performance of organic coatings is closely related with the dispersion of incorporated fillers. To check the dispersion status of graphene in WEP coating, the fracture surface morphologies of different coatings are examined by SEM, as shown in Fig. 5. Similar with previous report, the fracture surface of WEP coating presents several river-like cracks and pores, which results from the volatilization of water during the curing of coating [31]. After the incorporation of PSF, the fracture surface of PSF/WEP coating becomes denser than WEP coating, suggesting the addition of PSF can effectively reduce the generation of defects on the fracture surface (Fig. 5b). In case of G/WEP coating (Fig. 5c), there are still many pores and aggregation of graphene nanosheets on

the fracture surface owing to the poor dispersion and compatibility of graphene with water and epoxy. However, the aggregation of graphene nanosheets and pores for PSF@G/WEP coating are inhibited significantly when the graphene nanosheets are dispersed with PSF, which will be beneficial to slow down the diffusion of corrosive medium (Fig. 5d).

To investigate the protective performance of the coatings, electrochemical measurement was carried out. Fig. 6 presents the variation of the EIS results for WEP coating at different immersion times. After 2 days of immersion, Nyquist plot of WEP coating shows two capacitive arcs, in which the arc in high frequency corresponds to the coating response and the arc in the medium and low frequency is assigned to the charge transfer process at the metal/coating interface because of the penetration of corrosive medium (Fig. 6a) [32-34]. With the increasing immersion time (5~25 days), these two capacitive arcs reduces significantly, suggesting that electrochemical reactions are accelerated with the continuous water diffusion through the coating. In addition, the diffusion character appears at the low frequency, which is attributed to the diffusion of corrosive medium around the corrosion products on the substrate. At the same time, the impedance modulus at the lowest frequency ($Z_{f=0.01Hz}$) is an indicator of corrosion protection for organic coating [35]. The $Z_{f=0.01Hz}$ value of WEP coating also decreases gradually with increasing immersion time, which is about 10^5 Ω cm^2 after 20 days of immersion, indicating that WEP coating has lost the protective performance (Fig. 6b). Similarly, the phase angle at the high frequency of WEP coating varies from −60◦ to −36◦ with the prolonged immersion time (Fig. 6c). All variations in EIS results indicate that the WEP coating has lost its barrier property against the permeation of corrosive medium owing to the presence of large amounts of defects and pores.

For G/WEP coating (Fig. 7a-b), Nyquist plot presents one capacitive loop at 2 days of immersion and the $Z_{f=0.01Hz}$ value for G/WEP coating is 10^7 Ω cm^2. One broad time constant can be observed from the Bode plot (−Phase angle ~ Frequency), indicating the corrosion of the carbon steel is weak (Fig. 7c). As the immersion time elapsed (5 days), the uptake of corrosive medium makes the swell of the G/WEP coating, which increases the coating density to some extent. Although there is an increase in $Z_{f=0.01Hz}$ value ($10^{7.5}$ Ω cm^2), corrosive medium has penetrated into the coating/steel interface, leading to the corrosion of the substrate. Therefore, two capacitive arcs or time constants can be found from the Nyquist plot and Bode plot. However, after 20 days of immersion, the $Z_{f=0.01Hz}$ value of G/WEP coating decreases dramatically (bellow 10^6 Ω cm^2), indicating the failure of the coating. As comparison with WEP coating, the addition of graphene nanosheets improves the protective performance of the WEP coating to some extent. But the high conductivity of graphene nanosheets and the presence of aggregated graphene in WEP coating are inferior to the enhancement in the corrosion protection.

To overcome the above problem, PSF was used to improve the dispersion of graphene nanosheets in water. Thus, the effect of PSF on the corrosion protection of WEP coating is also investigated. As shown in Fig. 7d-f, Nyquist plots of PSF/WEP coating presents a broad capacitive arc in high and medium frequency and a diffusion field at the low frequency, in which the arc increases first and then shrinks with the increasing immersion time. Meanwhile, it can be observed that the $Z_{f=0.01Hz}$ value is about $10^{6.5}$ Ω cm^2 after 20 days of immersion, which is higher than those of WEP and G/WEP coating, indicating that the addition of PSF is beneficial to improve the corrosion resistance of

WEP coating. In case of PSF@G/WEP coating, the capacitive arc in Nyquist plot increases obviously during 5 days of immersion and decreases gradually with a further increase in immersion time (Fig. 7g). The $Z_{f=0.01Hz}$ value is about 10^7 Ω cm^2 after 20 days of immersion (Fig. h), which is similar with the previous reports [31, 36]. By comparison, among these four different coatings, PSF@G/WEP coating exhibits the best protective performance, which is attributed to the fact that the well dispersion of graphene with PSF improves the compatibility between graphene and WEP and eliminates the defects in the coating.

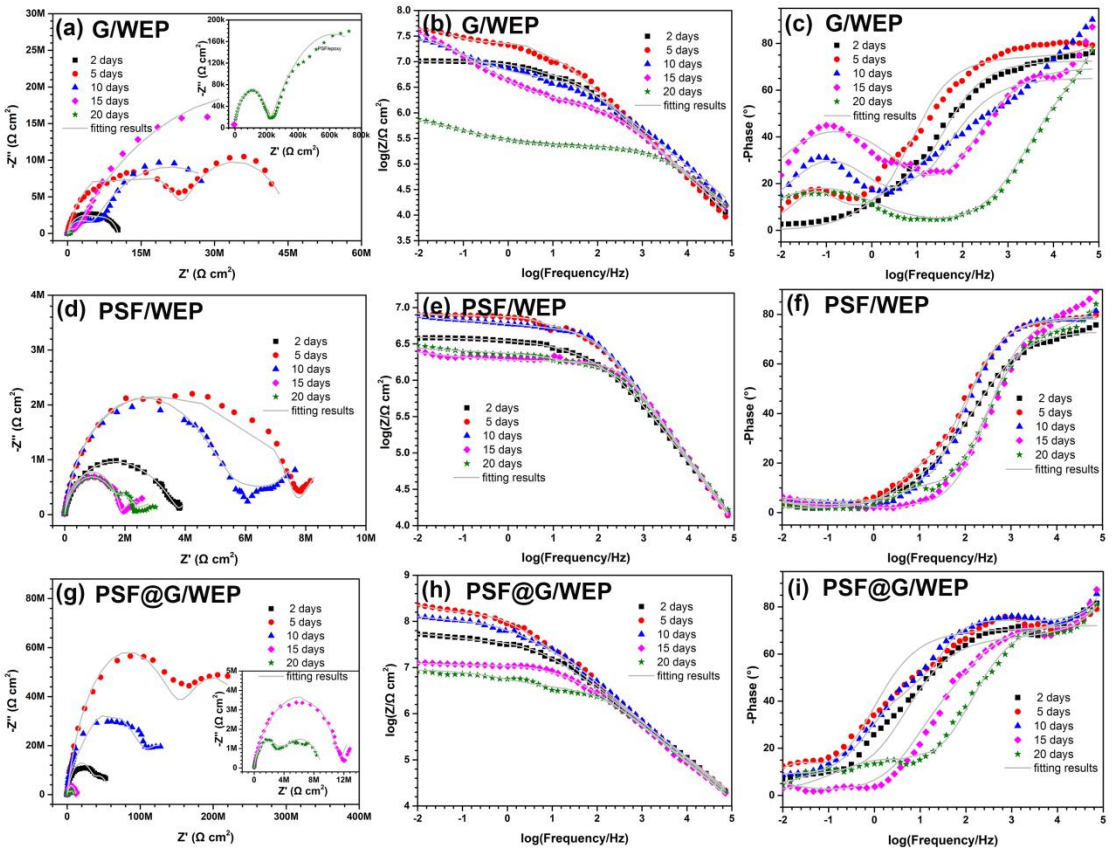

Figure 7. EIS results of different composite coatings (a-c) G/WEP coating, (d-f) PSF/WEP coating and (g-i) PSF@G/WEP coating, the scatter in the plot is experimental data and the solid line is the fitting results

To better understand the corrosion process of the coating/steel system, the EIS results are fitted with equivalent circuits shown in Fig. 8. For WEP coating, two time constants can be observed from the Bode plot at 2 days of immersion and the equivalent circuit in Fig. 8a can be used to fit the EIS result. In Fig. 8a, R_s is the solution resistance, CPE_c and R_c is assigned to the coating capacitance and coating resistance as well as CPE_{dl} and R_{ct} stands for the double layer capacitance and the charge transfer resistance [32]. With the increasing immersion time, the differential concentration of the corrosive medium in the coating disappears owing to the gradual absorption and the accelerated electrochemical reactions at the metal surface lead to the formation of a diffusive corrosion products layer [37]. As a result, equivalent circuit in Fig. 8b containing a diffusion component (Z_w) is applied to

fit the EIS results at this stage. For G/WEP coating, Bode plots during the whole process show two time constants (Fig.7c), thus the equivalent circuit in Fig. 8a is also appropriate to used. For PSF/WEP coating at 2 days of immersion, there is a broad time constant in the Bode plot owing to the weak corrosion of steel substrate (Fig.7f), which can be fitted by the equivalent circuit in Fig. 8a. The diffusion of corrosive medium in the coating or corrosion products appears with the prolonged immersion time, thus equivalent circuit in Fig. 8b can be used to fit the EIS results. As for PSF@G/WEP coating, two time constants are seen in the Bode plots during the whole immersion process (Fig. 7i), thus the EIS results can be fitted with the equivalent circuit in Fig. 8a. Further, the fitting results are almost in line with the experimental results, indicating the equivalent circuits used to fit the EIS results are appropriate. The appearance of the equivalent circuit in Fig. 8b implies that the corrosion of WEP, G/WEP and PSF/WEP coating/metal system is more severe than PSF@G/WEP coating.

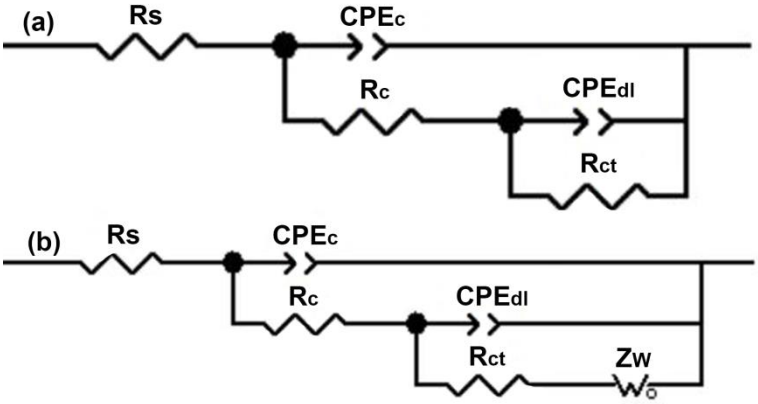

Figure 8. The equivalent circuit for fitting EIS results

In addition, the variation of the breakpoint frequency (f_b, it is a frequency value when the phase angle is −45°) could also be used to evaluate the protective performance of the coating. In general, f_b is closely related with the coating delamination area, which can be defined as the equation $f_b = K \cdot \frac{A_t}{A_0}$ ($K = \frac{1}{2}\rho\varepsilon\varepsilon_0$). In the equation, A_t is the disbonding area of the coating, A_0 is the total area of the sample, ρ is the electrical resistivity of the coating, ε is the dielectric constant of water in the coating, and ε_0 is the permittivity of vacuum [38-40]. The diffusion of corrosive medium into the coating/metal interface leads to the destruction of coating interfacial adhesion bonds, coating delamination and therefore direct contact of corrosive medium with metal surface [41]. It can be concluded from the equation that the breakpoint frequency increases by the increase of coating delamination. As shown in Fig. 9a, only two f_b values can be observed at 2 days and 5 days of immersion because the value of −phase angle for WEP coating is lower than 45° after 10 days of immersion, indicating the sever disbonding of the coating. For other coatings, f_b exhibits a shift to high frequency with the increasing immersion time, suggesting the gradual increase in disbonding area of the coating. Among them, PSF@G/WEP coating shows the lowest f_b value during 20 days of immersion, which indicates that the

addition of PSF@G can effectively reduce the coating delamination rate by inhibiting the diffusion of corrosive medium into the coating/metal interface and improve the barrier property of the coating.

Further, the coating resistance (R_c) obtained from the fitting process is also used to evaluate the barrier performance of coatings [31, 42]. As shown in Fig. 9b, the R_c value of all coatings decreases gradually with increasing immersion time. After the addition of graphene and PSF, the corrosion protection of the WEP coating is greatly enhanced and R_c value of G/WEP and PSF/WEP coatings is about one or two orders of magnitude higher than that of WEP coating. After the dispersion of graphene with PSF, R_c value of the PSF@G/WEP coating is higher than those of other three coatings, which is about three orders of magnitude higher than that of WEP coating. The reason is that the addition of PSF improves the dispersion of graphene in WEP and reduces the coating defects, which can prolong the diffusion path of water, O_2 and Cl^- in coating and enhance the labyrinth effect of the coating.

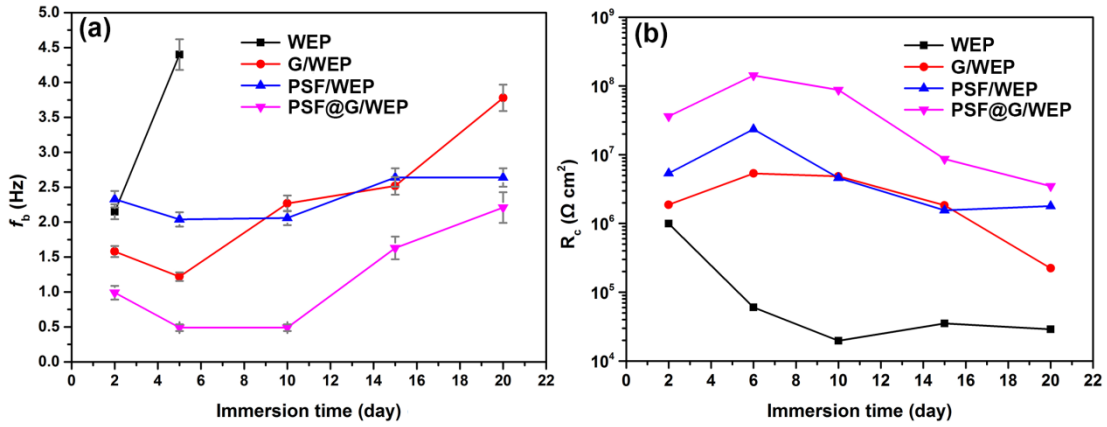

Figure 9. The variation of (a) breakpoint frequency and (b) coating resistance for different coatings as a function of immersion time

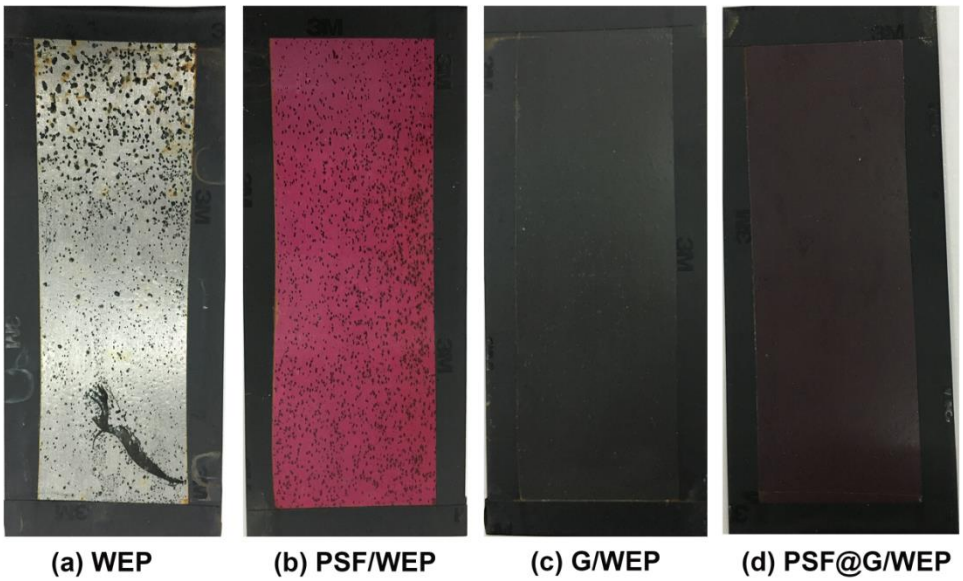

Figure 10. The images of different coating systems after 10 days of salt spray test

Salt spray test is also carried out to access the corrosion resistance of the different coatings. Results show that the surface of WEP and PSF/WEP coating present obvious rust spots after 10 days of salt spray test, G/WEP coating shows obvious blisters while there is no obvious corrosion observed at the surface of PSF@G/WEP coating. Based on the EIS results and salt spray test, it can be safe to conclude that PSF@G/WEP coating possesses the best protective performance.

4. CONCLUSIONS

The dispersion of graphene nanosheets in water was achieved by the assistance of surfactant–PSF. The adsorption free energy of the PSF@G system obtained from theoretical simulation was about –0.7 eV, suggesting the presence of strong π-π interaction between PSF and G. This dispersion technique could be beneficial to improve the compatibility of graphene and water-borne epoxy coatings and decrease th**e** coating defects. Long-term EIS results and salt spray test suggested that the impedance modulus and durability of the PSF@G/WEP coating were improved significantly since the addition of PSF@G could effectively block the coating defects and slow down the penetration of corrosive medium.

ACKNOWLEDGEMENTS

The authors gratefully acknowledged financial support provided by “One Hundred Talented People” of the Chinese Academy of Sciences (No. Y60707WR04); the Key Research Projects of Frontier Science, Chinese Academy of Sciences (QYZDY-SSW-JSC009), the Open Financial Grant from Qingdao National Laboratory for Marine Science and Technology (QNLM2016ORP0409), the Project of Science and Technology from State Grid Zhejiang Electric Power Company (5211NB16000F) and the Opening Project of State Key Laboratory of Explosion Science and Technology at Beijing Institute of Technology (Grant No.: KFJJ13-11M).

References

1. M.F. Craciun, S. Russo, M. Yamamoto and S. Tarucha, *Nano Today*, 6 (2011) 42-60.
2. K.S. Novoselov, S.V. Morozov, T.M.G. Mohinddin, L.A. Ponomarenko, D.C. Elias, R. Yang, I.I. Barbolina, P. Blake, T.J. Booth, D. Jiang, J. Giesbers, E.W. Hill and A.K. Geim, *Phys. Status Solidi B*, 244 (2007) 4106-4111.
3. C. Riedl, C. Coletti and U. Starke, *J. Phys. D: Appl. Phys.*, 43 (2010) 374009.
4. S. Ghosh, I. Calizo, D. Teweldebrhan, E.P. Pokatilov, D.L. Nika, A.A. Balandin, W. Bao, F. Miao and C.N. Lau, *Appl. Phys. Lett.*, 92 (2008) 151911.
5. A.A. Balandin, S. Ghosh, W. Bao, I. Calizo, D. Teweldebrhan, F. Miao and C.N. Lau, *Nano Lett.*, 8 (2008) 902-907.
6. H. Malekpour, K.H. Chang, J.C. Chen, C.Y. Lu, D.L. Nika, K.S. Novoselov and A.A. Balandin, *Nano Lett.*, 14 (2014) 5155-61.
7. D. Prasai, J.C. Tuberquia, R.R. Harl, G.K. Jennings and K.I. Bolotin, *ACS Nano*, 6 (2012) 1102–1108.
8. V. Berry, *Carbon*, 62 (2013) 1-10.

9. J.S. Bunch, S.S. Verbridge, J.S. Alden, A.M.v.d. Zande, J.M. Parpia, H.G. Craighead and P.L. McEuen, *Nano Lett.*, 8 (2008) 2458-2462.
10. B. Ramezanzadeh, S. Niroumandrad, A. Ahmadi, M. Mahdavian and M.H.M. Moghadam, *Corros. Sci.*, 103 (2016) 283-304.
11. W. Sun, L. Wang, T. Wu, M. Wang, Z. Yang, Y. Pan and G. Liu, *Chem. Mater.*, 27 (2015) 2367-2373.
12. O.C. Compton, S. Kim, C. Pierre, J.M. Torkelson and S.T. Nguyen, *Adv. Mater.*, 22 (2010) 4759-63.
13. E.G. B. Ramezanzadeh, M. Mahdavian, E. Changizi and M.H. Mohamadzadeh Moghadam *Carbon*, 93 (2015) 555-573.
14. M. Gao, Y. Pan, L. Huang, H. Hu, L.Z. Zhang, H.M. Guo, S.X. Du and H.J. Gao, *Appl. Phys. Lett.*, 98 (2011) 033101.
15. X. Wang, H. You, F. Liu, M. Li, L. Wan, S. Li, Q. Li, Y. Xu, R. Tian, Z. Yu, D. Xiang and J. Cheng, *Chem. Vapor Depos.*, 15 (2009) 53-56.
16. D. Wei, Y. Liu, Y. Wang, H. Zhang, L. Huang and G. Yu, *Nano Lett.*, 9 (2009) 1752-1758.
17. C. Zhao, B. Deng, G. Chen, B. Lei, H. Hua, H. Peng and Z. Yan, Nano Res., 9 (2016) 963-973.
18. Y. Si and E.T. Samulski, *Nano Lett.*, 8 (2008) 1679-1682.
19. P. Song, X. Zhang, M. Sun, X. Cui and Y. Lin, *RSC Adv.*, 2 (2012) 1168-1173.
20. W. Sun, L. Wang, T. Wu, Y. Pan and G. Liu, *Carbon*, 79 (2014) 605–614.
21. F. Zhang, X. Chen, R.A. Boulos, F.M. Yasin, H. Lu, C. Raston and H. Zhang, *Chem. Commun.*, 49 (2013) 4845-7.
22. H. Ma, Z. Shen, M. Yi, S. Ben, S. Liang, L. Liu, Y. Zhang, X. Zhang and S. Ma, *J. Colloid Interface Sci.*, 503 (2017) 68-75.
23. L. Zhang, Z. Zhang, C. He, L. Dai, J. Liu and L. Wang, *ACS Nano*, 8 (2014) 6663-6670.
24. J. Chen, W. Shi, Y. Chen, Q. Yang, M. Wang, B. Liu, Z. Tang, M. Jiang, D. Fang and C. Xiong, *Appl. Phys. Lett.*, 108 (2016) 073105.
25. S. Haar, M. Bruna, J.X. Lian, F. Tomarchio, Y. Olivier, R. Mazzaro, V. Morandi, J. Moran, A.C. Ferrari, D. Beljonne, A. Ciesielski and P. Samori, *J. Phys. Chem. Lett.*, 7 (2016) 2714-21.
26. X. Zhi, J. Liu, J. Xing and S. Ma, *Mater. Sci. Eng. A*, 603 (2014) 98-103.
27. J. Li, J. Cui, J. Yang, Y. Li, H. Qiu and J. Yang, *Compos. Sci. Technol.*, 129 (2016) 30-37.
28. Y. Li, Z. Yang, H. Qiu, Y. Dai, Q. Zheng, J. Li and J. Yang, *J. Mater. Chem. A*, 2 (2014) 14139-14145.
29. C. Wang, Y. Lan, W. Yu, X. Li, Y. Qian and H. Liu, *Appl. Surf. Sci.*, 362 (2016) 11-19.
30. S. Perumal, H.M. Lee and I.W. Cheong, *J. Colloid Interface Sci.*, 497 (2017) 359-367.
31. S. Qiu, W. Li, W. Zheng, H. Zhao and L. Wang, *ACS Appl. Mater. Interfaces*, 9 (2017) 34294-34304.
32. Y. Liu and Y. Chen, *Int. J. Electrochem. Sci.*, *13* (2018) 530-541.
33. M. Yeganeh and M. Saremi, *Prog. Org. Coat.*, 79 (2015) 25-30.
34. M.F. Montemor, D.V. Snihirova, M.G. Taryba, S.V. Lamaka, I.A. Karsonakis, A.C. Balaskas, G.C. Kordas, J. Tedim, A. Kuznetsova, M.L. Zheludkevich and M.G.S. Ferreira, *Electrochim. Acta*, 60 (2012) 31.
35. M. Cui, S. Ren, S. Qin, Q. Xue, H. Zhao and L. Wang, *Corros. Sci.*, 131 (2018) 187-198.
36. C. Liu, P. Du, H. Zhao and L. Wang, *ACS Appl. Nano Mater.*, 1 (2018) 1385-1395.
37. F. Mansfeld and M.W. Kendig. Laboratory Corrosion Tests and Standards. *ASTM International*, 1985.
38. M. Cui, S. Ren, J. Chen, S. Liu, G. Zhang, H. Zhao, L. Wang and Q. Xue, *Appl. Surf. Sci.*, 397 (2017) 77-86.
39. X. Liu, J. Xiong, Y. Lv and Y. Zuo, *Prog. Org. Coat.*, 64 (2009) 497-503.
40. H.P. Hack, *J. Electrochem. Soc.*, 138 (1991) 33.
41. B. Ramezanzadeh, G. Bahlakeh, M.M. Moghadam and R. Miraftab, *Chem. Eng. J.*, 335 (2018) 737-755.

42. Y. Li, Z. Yang, H. Qiu, Y. Dai, Q. Zheng, J. Li and J. Yang, *J. Mater. Chem. A*, 2 (2014) 14139-14145.